Swansea University
Prifysgol Abertawe

Cronfa
Setting Research Free

Cronfa - Swansea University Open Access Repository

This is an author produced version of a paper published in:
Electrochimica Acta

Cronfa URL for this paper:
http://cronfa.swan.ac.uk/Record/cronfa51519

Paper:
Gannon, W. & Dunnill, C. (2019). Raney Nickel 2.0: Development of a high-performance bifunctional electrocatalyst. *Electrochimica Acta*, 134687
http://dx.doi.org/10.1016/j.electacta.2019.134687

This item is brought to you by Swansea University. Any person downloading material is agreeing to abide by the terms of the repository licence. Copies of full text items may be used or reproduced in any format or medium, without prior permission for personal research or study, educational or non-commercial purposes only. The copyright for any work remains with the original author unless otherwise specified. The full-text must not be sold in any format or medium without the formal permission of the copyright holder.

Permission for multiple reproductions should be obtained from the original author.

Authors are personally responsible for adhering to copyright and publisher restrictions when uploading content to the repository.

http://www.swansea.ac.uk/library/researchsupport/ris-support/

Journal Pre-proof

Raney Nickel 2.0: Development of a high-performance bifunctional electrocatalyst

William J.F. Gannon, Charles W. Dunnill

PII: S0013-4686(19)31558-0

DOI: https://doi.org/10.1016/j.electacta.2019.134687

Reference: EA 134687

To appear in: *Electrochimica Acta*

Received Date: 8 May 2019

Revised Date: 29 July 2019

Accepted Date: 12 August 2019

Please cite this article as: W.J.F. Gannon, C.W. Dunnill, Raney Nickel 2.0: Development of a high-performance bifunctional electrocatalyst, *Electrochimica Acta* (2019), doi: https://doi.org/10.1016/j.electacta.2019.134687.

This is a PDF file of an article that has undergone enhancements after acceptance, such as the addition of a cover page and metadata, and formatting for readability, but it is not yet the definitive version of record. This version will undergo additional copyediting, typesetting and review before it is published in its final form, but we are providing this version to give early visibility of the article. Please note that, during the production process, errors may be discovered which could affect the content, and all legal disclaimers that apply to the journal pertain.

© 2019 Published by Elsevier Ltd.

[a]Energy Safety Research Institute, Swansea University, SA1 8EN, UK

Abstract

As a catalytic coating for alkaline electrolysis Raney Nickel is one of the most efficient materials discovered, based largely on the activity of nickel and the porosity of the alloy after leaching. This study improves the electrochemical and corrosion performance of the coating for both hydrogen and oxygen evolution in alkaline water-splitting electrolysis through the use during electrodeposition of a sacrificial stainless-steel counter electrode. Analysis using energy dispersive X-ray (EDX) and scanning electron microscopy (SEM) revealed that the although the elemental make-up is largely similar, the morphology is transformed. Through measurements of the electrochemical surface area (ECSA) after long-term intermittent ageing it was found that the surface area was increased by a factor of six. Assessments and comparisons of the electrochemical performance using 3-electrode chronopotentiometry confirm this is one of the most active bifunctional coatings known.

Keywords: alkaline, electrolysis, bifunctional, raney nickel

Journal Pre-proof

1. Introduction

Enough solar energy reaches the Earth's surface to meet our current energy consumption 10,000 times over[1, 2]. Despite this, (according to the World Bank) fossil fuels still make up 80 % of total energy consumption. Renewable energy offers the opportunity to greatly reduce this figure, but one of its greatest drawbacks is intermittency. Worse still, when renewable energy is available, its timing may not coincide with peak energy. To this end, the storing of energy as hydrogen gas decouples supply from demand, and offers great potential to permit both developed and developing nations to reduce or avoid future dependency on fossil fuel, as well as achieving great efficiency savings in energy transport and distribution. There are many concurrent branches of research focussed on energy conversion to hydrogen, for example photocatalytic water-splitting[3–5] and artificial photosynthesis[6, 7], and to this the addition of a low-cost, reliable, efficient electrolyser that can utilize highly variable electrical input would be of great benefit[8, 9]. Such a device could on a small-scale be connected directly to wind turbines and solar farms, thereby introducing energy conversion, buffering and storage into the energy network at the earliest opportunity, and gaining efficiencies that would otherwise be lost due to electrical management and transport[10].

In this study a comparison will be made between two different types of electrodeposited Raney nickel, as listed in Table 1. Coating Raney 1 is based on that refined by I. Herraiz-Cardona *et al.*[11], itself based on earlier work[12], and ultimately based on processes which are widely used in the nickel plating industry, and were first formulated by Professor Oliver P. Watts in 1916[13]. Coating Raney 2 is new, and differs only in the choice of counter electrode. It is our aim to present evidence for the profound and beneficial effects this produces for the performance and longevity of the coating.

Coating	Substrate	Coating	Electrodeposition Counter-electrode
Raney 1	316SS	Ni/Zn	Graphite rod
Raney 2	316SS	Ni/Zn	316SS

Table 1: The two electrolcatalytic coatings compared in this study, which differ only in the choice of counter-electrode used during electrodeposition. 316SS = 316-grade stainless steel.

Raney Nickel has been studied extensively since its discovery in 1926, and is made by dissolving nickel in molten aluminium, followed by the addition of zinc or chromium whilst quenching. Electrodeposition methods have been investigated commercially since the 1950's,[14] and in academia since the 1980's,[12, 14–17] in addition to other methods such as pressed powders and plasma spraying[18]. Although typically investigated for hydrogen evolution,[11, 19–25] as well as in combination with non-abundant compounds,[26–28] the coating is also known to perform well for oxygen evolution[29, 30].

In the field of alkaline water-splitting electrolysis, it is recognised that insufficient attention has been paid to long-term system performance when driven from variable and discontinuous renewable energy sources. To quote from Chapter 8 of 'Hydrogen Production by Electrolysis' (edited by Agata Godula-Jopek) "it seems fair to say that the

*Corresponding author
Email address: c.dunnill@swansea.ac.uk (Charles W Dunnill)

this highly practical area of research by focussing on the performance of electrocatalytic coatings when subjected to a simulated intermittent environment, whereby ageing may be achieved over reduced time-scales[32].

In very long-term studies completed between 1989 and 1994, some running to more than 10,000 hours, it was reported by Divisek *et al.* that a Ni/Al Raney Nickel cathode experienced 'complete destruction' when subjected to electrolyser shutdown[33], forcing the authors to conclude that "the only catalytic coating resistant to depolarization consists of the metals of the Pt group". A Raney coating based on zinc fared little better, and in bi-polar operation "to avoid major deterioration, the cells were polarized with a protective current"[34], i.e. a permanent back-up power supply was required to permit the electrolyser to cope with intermittent usage. Although some protective effect was discovered via the incorporation of Mo into the coating, this protection was only temporary.

When the power input to a water-splitting electrolyser is interrupted, the electrodes will have stored charge within them in the form of capacitances, adsorbed species, ionisation changes and as chemically altered compounds. As the electrodes subsequently discharge this can lead to corrosion currents that will selectively leach out vital components of the catalytic coating. If this process continues far enough, it can lead to the sort of 'complete destruction' reported by Divisek *et al*[33]. The possibilities for discharge currents are greater in bipolar electrode stacks, because the presence of electrolyte side-channels running through the stack mean that there are many possible electrolyte pathways by which currents can flow. Some of these will be connecting electrodes at greatly differing voltages, which could permit the corrosion of components which would otherwise be stable. Despite this, the current study focuses on a monopolar design, due to its simplicity.

Corrosion will also be considerably different at the anode and cathode. Since metals form positively charged ions in solution, their dissolution is associated with loss of electrons i.e. anodic oxidation. During continuous operation, such as in a commercial electrolyser, the water-splitting reactions dominate, and the corrosion rate of a well-designed electrode can be minimal. During unprotected discharge, reverse currents can flow, and it is therefore the cathode that can experience the greatest rate of corrosion,[35, 36] especially of components that have the most negative electropotential such as zinc, which are therefore the most stable in solution. Charting what changes occur, how these affect the performance of the electrocatalytic coating, and how they may potentially be avoided is of great interest to the goal of harnessing intermittent renewable energy to power the hydrogen economy.

$$\mathrm{H_2O + e^- \longrightarrow H_{ads} + OH^-} \qquad \text{(Volmer)}$$
$$\mathrm{H_{ads} + H_2O + e^- \longrightarrow H_2(g) + OH^-} \qquad \text{(Heyrovsky)}$$
$$\mathrm{H_{ads} + H_{ads} \longrightarrow H_2(g)} \qquad \text{(Tafel)}$$

where $\mathrm{H_{ads}}$ stands for an uncharged hydrogen atom adsorbed onto the surface of the electrode material. The shape of the plot of log of current versus potential (a Tafel plot) will vary depending upon which of the reactions is the rate-limiting step, as described in Table 2[40]. Assuming therefore that any of the transitions of slope can be observed experimentally, the rate-limiting step could thereby be surmised with a high degree of confidence.

Rate-Limiting Step	**Tafel slopes** (in $\mathrm{mV\,dec^{-1}}$)
Volmer	$0 \rightarrow -120$
Heyrovsky	$0 \rightarrow -40 \rightarrow -120$
Tafel	$0 \rightarrow -30 \rightarrow -\infty$

Table 2: Theoretical Tafel slopes observed for HER

For the Oxygen Evolution Reaction (OER) in alkaline media, the reaction is multi-step and irreversible. There are many (broadly similar) possible reaction mechanisms by which it may proceed, and one such scheme is shown below:

$$\mathrm{OH^- \longrightarrow OH_{ads} + e^-} \tag{1}$$
$$\mathrm{OH_{ads} + OH^- \longrightarrow O_{ads} + H_2O + e^-} \tag{2}$$
$$\mathrm{O_{ads} + OH^- \longrightarrow OOH_{ads} + e^-} \tag{3}$$
$$\mathrm{OOH_{ads} + OH^- \longrightarrow OO^-_{ads} + H_2O} \tag{4}$$
$$\mathrm{OO^-_{ads} \longrightarrow O_2(g) + e^-} \tag{5}$$

There are four different types of adsorbed species (O, OH, OOH and $\mathrm{OO^-}$) and four of the steps involve electron transfer, which means that the reactions can draw electrical energy from the potential on the electrode. Steps 4 and 5 are often combined as a single step, but there is good evidence to suggest that they occur as two separate steps above pH 11[41], which is where practical alkaline electrolysers operate. The resulting theoretical range of slope transitions for OER are presented in Table 3[40].

Rate-Limiting Step	**Tafel slopes** (in $\mathrm{mV\,dec^{-1}}$)
Reaction 1	$0 \rightarrow 120$
Reaction 2	$0 \rightarrow 30 \rightarrow 120$
Reaction 3	$0 \rightarrow 21 \rightarrow 40 \rightarrow 120$
Reaction 4	$0 \rightarrow 22 \rightarrow 30 \rightarrow 60 \rightarrow 120 \rightarrow \infty$
Reaction 5	$0 \rightarrow 22 \rightarrow 120$, or $0 \rightarrow 40 \rightarrow 120$

Table 3: Theoretical Tafel slopes observed for OER

Journal Pre-proof

effects and bubbles[8]. Nevertheless, useful conclusions can still be drawn from modest amounts of information.

2. Method

2.1. Electrodeposition of Raney Nickel

All procedures were conducted in standard laboratory 100 ml beakers. Such beakers are large enough to accommodate up to two 4 cm × 4 cm paddle-shaped stainless-steel electrodes, as shown in Figure 1. For Raney 2 the graphite rod counter electrode is exchanged for one made from 316-grade stainless-steel, which is partially consumed during the deposition, thereby progressively altering the composition of the coating.

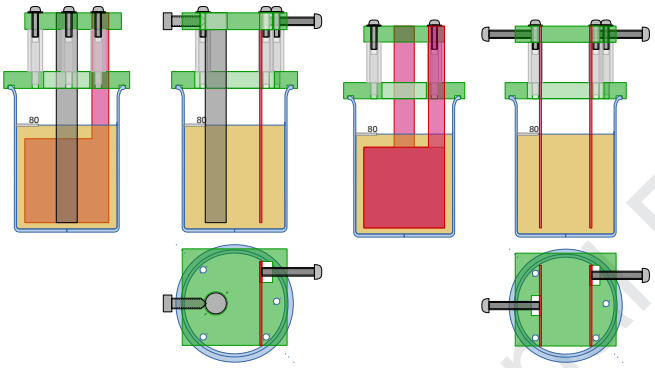

(a) Raney 1 deposition (b) Raney 2 deposition

Figure 1: Mechanical drawings of the electrodeposition chambers for a) Raney 1, which employs a graphite rod counter-electrode and b) Raney 2, which employs a 316-grade stainless steel counter-electrode. Both chambers were primarily constructed using laser cut acrylic components, plus a standard 100 ml laboratory beaker

Pretreatment. The 4 cm × 4 cm stainless-steel electrode was degreased in hot 25 wt% NaOH for 1 minute, then submerged in 18 wt% HCl for 1 minute at room temperature, before being placed in 70 wt% H_2SO_4 for 3 minutes at an anodic current of 108 mA m^{-2}. Lastly the electrode was placed in a Nickel Strike solution consisting of 240 g l^{-1} $NiCl_2 \cdot 6\,H_2O$ and 120 ml l^{-1} HCl for 5 minutes at a cathodic current of −26.8 mA cm^{-2}. Between each step the electrode was rinsed with deionised water, and the air-exposure time between each step kept to a minimum. At this point the electrode was observed to be covered in a thin, adherent coating of nickel that is able to act as a base for any subsequent functional coatings[21].

Functional Coating. The electrode was immersed in a modified Watt's Bath consisting of 330 g l^{-1} $NiSO_4 \cdot 6\,H_2O$, 45 g l^{-1} $NiCl_2 \cdot 6\,H_2O$, 37 g l^{-1} H_3BO_3 and 20 g l^{-1} $ZnCl_2$ at 50 °C for 60 minutes at a cathodic current of −50 mA cm^{-2}. During this procedure the shown in Figure 2 (left).

2.2. Electrochemical Surface Area (ECSA)

The ECSA is an estimate of the real surface area of the electrode, and it can be very much larger than its geometric area. Based on the assumption that the Helmholtz double-layer is very thin, the ECSA should be proportional to the double-layer capacitance (C_{DL}) and can therefore be determined by measuring the currents required to charge and discharge the electrode. In essence, this requires finding a region where all other currents are minimised, specifically Faradaic currents (which are related to water-splitting) and redox currents (which are related to changes of oxidation state).

The voltage was cycled by ±50 mV, at various scan rates, in a non-Faradaic region, usually around open-circuit potential (OCP). Before each change of scan direction, the voltage was held for 10 seconds to allow diffusion gradients to disperse[42]. Assuming that all of the current goes towards charging and discharging the double-layer capacitance, the charging current will be given by:

$$i_c = \nu C_{DL} \tag{1}$$

where ν is the scan-rate. Unfortunately, the values of capacitance observed in this study were often so large that the current had not stabilised within the measurement window. Therefore a method was developed that performed a best-fit of an RC-network model to the current waveforms. This method also has a very good ability to reject artefacts that are present on the waveforms.

Once the double-layer capacitance has been determined, the ECSA can be calculated by comparing this value to that expected for a flat plate, namely the specific capacitance C_S, which in 1 M NaOH is widely-accepted to be 0.040 mF cm^{-2}[43].

$$ECSA = C_{DL}/C_S \tag{2}$$

Finally, the roughness factor (RF) was determined by dividing the ECSA by the geometric surface area.

2.3. Three electrode experiments

All 3-electrode experiments were conducted on an Ivium n-Stat potentiostat, connected to a laminated electrolytic cell, chiefly comprised of laser-cut acrylic plastic, as shown in Figure 2 (right), which is similar to previous test cells[44].

The exposed area of the working electrode (WE) was 3 cm × 3 cm, the counter electrode was a 316 stainless-steel plate (of which 6 cm × 6 cm was exposed), and the reference electrode (RE) was a commercial design involving a Ag/AgCl wire suspended in 3 M KCl. The distance between working and counter electrodes was approximately

Journal Pre-proof

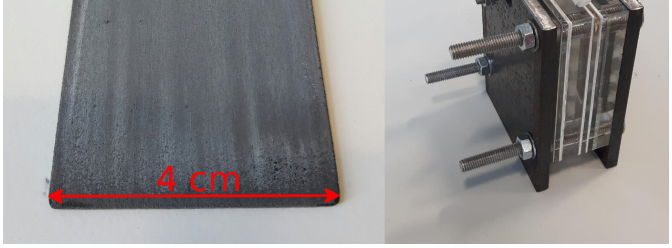

Figure 2: Raney 2 electrode (left) and as assembled into the three-electrode cell (right)

15 mm. The electrolyte was 0.5 M NaOH (standard reagent grade) and deionised water was used throughout. Before each experiment the RE was checked against a standard calomel electrode (SCE), and the electrolyte was bubbled with nitrogen for 10 minutes to reduce dissolved oxygen. All experiments were conducted at laboratory ambient temperature, which was 20 ±1 °C.

2.4. Overpotentials

Overpotentials were calculated with reference to the chart of potentials at pH 13.7, as shown in Figure 3.

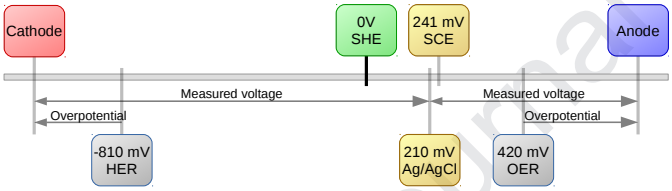

Figure 3: Diagram of relevant potentials at pH 13.7 (to scale)

It is important to clarify that the diagram shows potentials (for which the symbol E will be used), whereas experimentally we are restricted to measuring voltages (i.e. the difference between two potentials, for which the symbol V will be used). The standard potential for the hydrogen evolution reaction at pH 0 is 0 V, since this is a description of the standard hydrogen electrode (SHE), which is used to define 0 V. As the pH becomes more alkaline, this potential will shift by −59.1 mV for every unit on the pH scale, therefore in 0.5 M NaOH at pH 13.7, the standard potential for the HER is:

$$E_{0,HER} = 0\ V - 13.7 \times 59.1\ mV = -810\ mV \quad (3)$$

The standard potential for the OER will be 1.23 V higher than this, at 420 mV. The Ag/AgCl reference electrode will remain at 210 mV *vs.* SHE, therefore to obtain overpotentials from our measured voltages, we use:

$$\eta_{OER} = V_{anode} - iR_S - (E_{0,OER} - E_{AgAgCl}) \quad (4)$$

the SCE, which is understandable given the basic conditions under which it was operating, and the regularity of the servicing it underwent. Therefore, before each experiment an offset voltage to the SCE was measured and used to correct for drift of the reference electrode.

2.5. Accelerated Ageing

All two-electrode accelerated ageing experiments were conducted on an Ivium n-Stat potentiostat, connected to a laminated electrolytic cell of a similar design to that in Figure 2. A Zirfon^{TM} membrane was used to keep the evolved gases separate, and the distance between electrodes was approximately 30 mm. Each cycle consisted of 2 minutes at 200 mA cm^{-2}, followed by 2 minutes at open-circuit. Each experiment consisted of 2000 cycles, totalling 5.5 days. The electrolyte was not circulated and consisted of 2.5 l of 1 M NaOH stored in a displacement tube. The reference electrode was not present, since it cannot withstand prolonged exposure to NaOH.

2.6. Sputter coating

The platinum sputter coating was performed on a Quorum Q150T S, using a 0.3 mm thick 99.99 % pure platinum target at a sputter current of 30 mA for 60 seconds onto a 0.9 mm thick 316 grade stainless-steel plate.

2.7. Electron Microscope

Scanning electron microscope (SEM) imaging and energy dispersive spectroscopy (EDX) were performed on an Oxford Instruments AZtecOne spectrometer attached to a Hitachi TM3030 table top microscope. To achieve coincident electromicrographs before and after ageing, a small stylus mark was made on the electrode away from the coated area. This was used to zero the axes, prior to moving the stage a fixed distance and visually locating the previously examined location.

3. Results: Oxygen Evolution

The peak voltages of the 2-electrode cells containing the Raney nickel anodes during the accelerated ageing tests were as shown in Figure 4. The trend line shows the results after the data have been manipulated to correct for temperature variations, and to introduce some smoothing. The cell with the Raney 1 coating shows a gradual but consistent degradation in performance, finishing the experiment about 150 mV higher. The cell with the Raney 2 coating had more problems with consistency (which were due to the presence of air-locks), but generally lower voltages throughout.

Journal Pre-proof

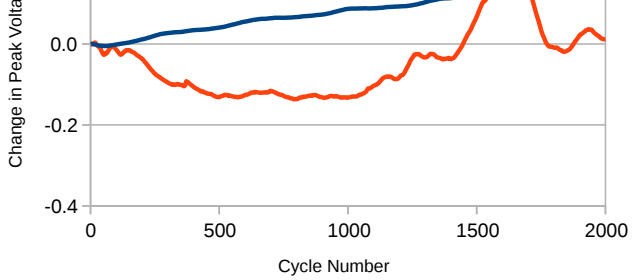

Figure 4: Peak OER cell voltages over 2000 cycles of 2 minutes on 2 minutes off accelerated ageing

The anodes were analysed in isolation in the 3-electrode cell, and the results were as shown in Figure 5. Both coatings exhibit an improvement after ageing, which implies that the ageing process brings about changes in the coating which are beneficial for oxygen evolution. The improvement for Raney 2 is much larger than that for Raney 1, but this may have been due to partial oxidation of the electrode prior to ageing. If so the results serve to highlight how the coating can recover its performance through normal usage. After ageing, the Raney 2 coating is able to outperform Raney 1 by over 50 mV, which equates to a 300-fold increase in current density at an overpotential of 0.3 V. The results are included for 1M KOH to illustrate the effect of changing the electrolyte. They show that this extends the useful range of the electrode by another order of magnitude. All five plots show a region which appears to be parallel to 30 mV dec^{-1}, therefore it is expected that either OER Reaction 2 or Reaction 4 is the rate-limiting step.

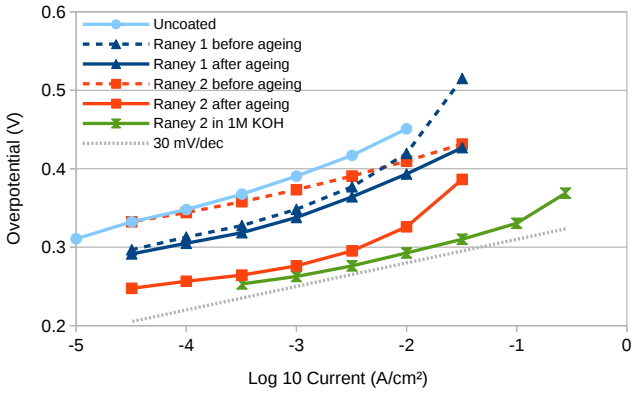

Figure 5: Tafel plots for OER before and after ageing

The ECSA measurements are as shown in Table 4. They show that as deposited Raney 2 has a surface area approximately 3 times larger than that of Raney 1, and normal usage. At a roughness factor of 885, the Raney 2 anode is successfully exposing 1 m^2 of reaction surface to the electrolyte for each 11 cm^2 of electrode. The capacitance measured for the 3 cm × 3 cm surface is nearly 3 Farads, thereby indicating that the electrode can be classified as a super-capacitor. It is useful confirmation of the high capacitances that can be created using the Helmholtz double-layer.

Anode		Capacitance	ECSA	RF
Raney 1	**As deposited**	0.29 F	797 cm^2	89
	After ageing	1.08 F	3008 cm^2	334
Raney 2	**As deposited**	0.75 F	2077 cm^2	231
	After ageing	2.87 F	7968 cm^2	885

Table 4: ECSA measurements for 3 cm × 3 cm Raney Nickel anodes before and after accelerated ageing

4. Results: Hydrogen Evolution

The peak voltages of the 2-electrode cells containing Raney nickel cathodes during the accelerated ageing tests were as shown in Figure 6. The trend line shows the results after the data have been manipulated to correct for temperature variations, and to introduce some smoothing. The performance of both cells decreased by approximately 200 mV, although this could be due to any component of the system, such as the stainless-steel anode or the gas-separation membrane, and not necessarily the cathode.

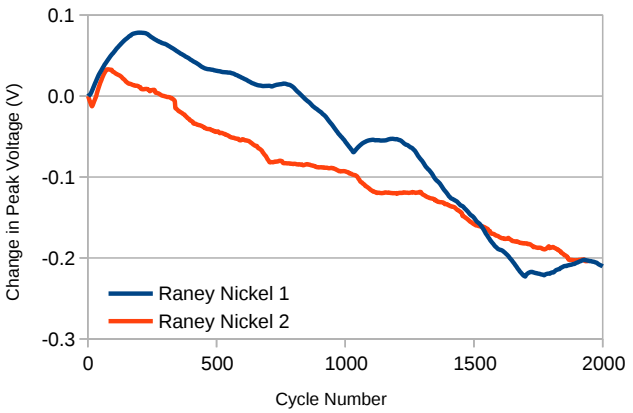

Figure 6: Peak HER cell voltages over 2000 cycles of 2 minutes on 2 minutes off accelerated ageing

The Raney 2 cathode was also analysed over 24 hours of chronoamperometry at a cell voltage of −2.5 V, with the results as presented in Figure 7. Note that the left-hand y-axis has been inverted to assist in highlighting the correlation between cell current and temperature, which

Journal Pre-proof

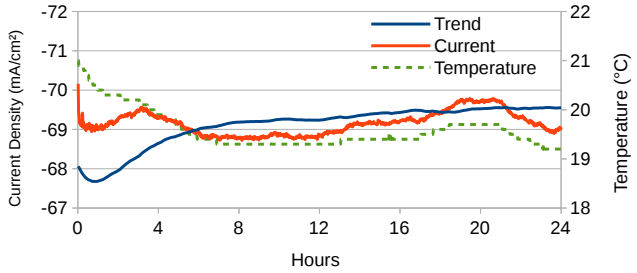

Figure 7: Chronoamperometry for HER of Raney 2 over 24 hours at $-2.5\,\mathrm{V}$

The cathodes were analysed in the 3-electrode cell, as shown in Figure 8, and in greater detail in Figure S1. Both Raney 1 and 2 improve with ageing, with Raney 2 showing the greater increase in performance. Both coatings show a significant improvement in performance over the uncoated electrode, amounting to an increase in excess of 10,000-fold in current density. Both coatings also showed a consistent tendency to produce slightly negative overpotentials at current densities below $3.2\,\mathrm{mA\,cm^{-2}}$, which is not fully explained.

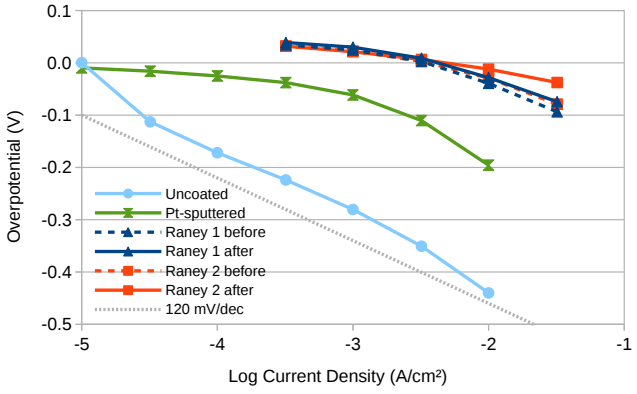

Figure 8: Tafel plots for HER before and after accelerated ageing

The results for a Pt-sputtered plate are also included, which serve to underline how a smooth, expensive material can be outperformed comprehensively by a much lower-cost material with a sufficiently large surface area. The Pt-sputtered plate shows a transition in slope from $40\,\mathrm{mV\,dec^{-1}}$ to $120\,\mathrm{mV\,dec^{-1}}$, therefore it is expected that the Heyrovsky reaction is the rate-limiting step. Unfortunately there are not enough points to draw the same conclusion for the Raney Nickel coatings, since there are in general too many bubbles above $32\,\mathrm{mA\,cm^{-2}}$ for Tafel analysis to be reliable.

The ECSA measurements were as shown in Table 5. They confirm that as deposited Raney 2 has a surface it 6 times more surface area. These results correlate well with the changes observed during the Tafel analysis above. This surface area is of immense utility in helping the coating to achieve the high current densities observed in the HER Tafel analysis. The ECSA measurement for the Pt-sputtered electrode has been included for comparison, and as a consistency check since because it is flat, it should produce a roughness factor which is close to unity.

Cathode		Capacitance	ECSA	RF
Raney 1	**As deposited**	0.19 F	$528\,\mathrm{cm^2}$	59
	After ageing	0.21 F	$580\,\mathrm{cm^2}$	64
Raney 2	**As deposited**	0.66 F	$1829\,\mathrm{cm^2}$	203
	After ageing	1.38 F	$3825\,\mathrm{cm^2}$	425
Pt-sputtered		2.2 mF	$6.2\,\mathrm{cm^2}$	0.7

Table 5: ECSA measurements for $3\,\mathrm{cm} \times 3\,\mathrm{cm}$ Raney Nickel cathodes before and after accelerated ageing

5. Characterisation

The Raney Nickel electrodes were characterised using SEM and EDX, for both HER and OER, and before and after accelerated ageing. Typical SEM images at 500× magnification for Raney 1 and 2 as deposited are shown in Figure 9.

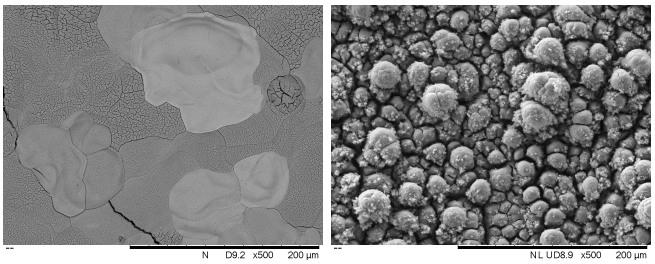

(a) Raney 1 (b) Raney 2

Figure 9: SEM images of the two Raney Nickel coatings as deposited at 500× magnification

The images reveal that the morphology of the Raney nickel coating has been greatly affected by the change of counter electrode. The Raney 1 coating has a relatively flat, cracked paving appearance, with many areas appearing to be almost solid. By contrast the Raney 2 coating has a much more three-dimensional appearance that suggests it will have a larger surface area, and be better able to engage with the electrolyte. This is borne out by the better electrical performance of the coating prior to the ageing tests. A comparative view of the Raney 2 coating before and after accelerated ageing as cathode is shown in Figure S2 at 500× magnification. The micrographs confirm that no deterioration of the coating is visible.

nickel is being lost, however once the figures are adjusted to exclude oxygen (as shown in Figure 10b), it becomes clear that the percentages of Ni, Zn, Cu and Fe are remaining constant, with just a small increase for carbon. This is in contradiction of comparable results obtained by Divisek *et al.* where a large loss of zinc from the anode was observed, although it was stated that this had little effect on its performance[34]. It has been confirmed that nickel electrodes gradually dissolve when used for oxygen evolution, as the $Ni(OH)_2/NiOOH$ film produces soluble Ni(II) species[45], and these results produce nothing in contradiction with this finding.

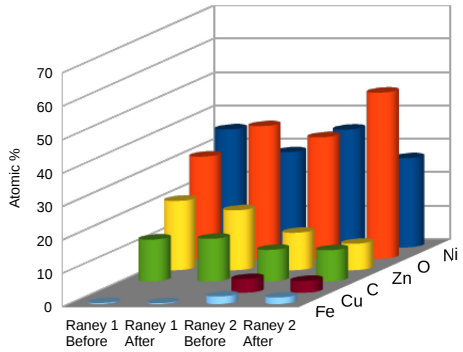

(a) including oxygen

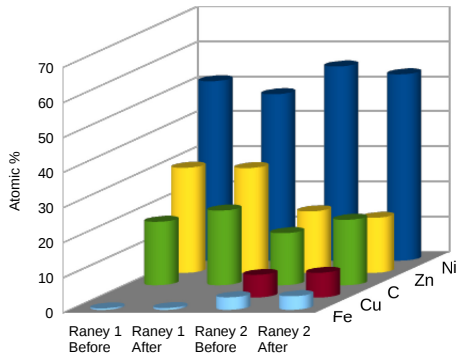

(b) excluding oxygen

Figure 10: EDX results before and after accelerated ageing of Raney nickel anodes

The EDX results for the Raney nickel cathodes are shown in Figure 11. At the cathode the opposite effect is observed, with a decrease in the level of oxygen after ageing. If oxygen and copper are numerically excluded from the analysis, nickel abundance is observed to increase, largely due to the loss of zinc. Nevertheless, the marked increase in the level of copper is quite noticeable. In fact, places on the cathodes were discovered at which the surface was more than 60 at% copper. For Raney 2 the source of this copper before ageing is speculated to be the sacrificial stainless-steel counter electrode used during deposi-

increased for both cathodes, and the source of this copper is speculated to be the stainless-steel anode used during the accelerated ageing experiments. This will have released small amounts of copper into the electrolyte, which are then preferentially deposited and concentrated onto the surface of the cathode.

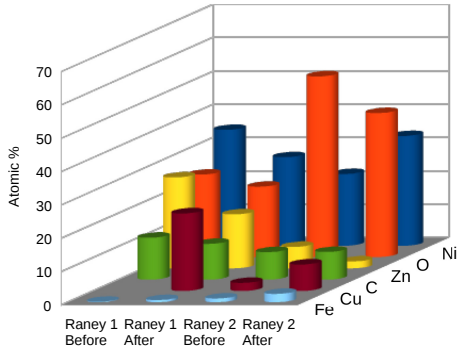

(a) including oxygen

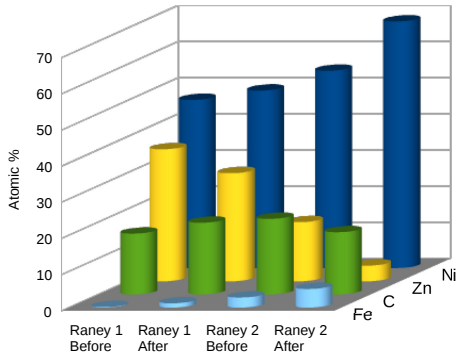

(b) excluding oxygen and copper

Figure 11: EDX results before and after accelerated ageing of Raney nickel cathodes

According to published official standards, 316-grade stainless-steel does not contain any copper. To investigate this, EDX experiments were conducted on samples from two separate suppliers, and small amounts of copper between 1 and 1.6 wt% were observed in both. This result is interesting because it appears to highlight the extent to which sources of copper contamination can become highly concentrated on the surface of the cathode during use.

6. Performance Comparisons

In order to assess how the Raney 2 electrodeposited coating compares with other bi-functional catalysts, a small survey was conducted to find other recently-published bi-functional catalysts for water-splitting in alkaline conditions, as shown in Table 6.

NiCu	1 M KOH	n/s	[50]
NiSe-NF	1 M KOH	n/s	[51]
NiS/Ni	1 M KOH	n/s	[52]
CoP-MNA	1 M KOH	n/s	[37]

Table 6: Nickel catalysts reported by Herraiz-Cardona *et al.* n/s = not specified, but presumed to be room temperature.

The results of these comparisons are shown in Figures S3 and S4, where the results chosen for Raney 2 are those produced in 1 M KOH. They show that for hydrogen evolution the Raney 2 coating compares extremely favourably with recently published bi-functional catalysts, and is near the middle for oxygen evolution. However, when both are combined the coating is second only to the world-leading FeP/Ni_2P, which is a coating that features a more complicated deposition method involving chemical vapour deposition within a tube furnace. The performance of the coating has also been compared with various results reported by Herraiz-Cardona *et al.* and Solmaz *et al.* There are a selection of materials with which to compare, as listed in Table 7, with the results as shown in Figures S5 and S6.

Name	Electrolyte	Temp	Ref
Ni/Zn	30 wt% KOH	50 °C	[11]
NiCo-2	30 wt% KOH	30 °C	[23]
Ni-Hcd	30 wt% KOH	50 °C	[53]
NiR	30 wt% KOH	30 °C	[22]
NiCo/Zn	30 wt% KOH	30 °C	[21]
Cu/NiCuZn	1 M KOH	RT	[24]
MS/Ni/NiZn-Pt	1 M NaOH	298 K	[25]
Cu/NiNiZn-PtRu1	1 M KOH	298 K	[26]
Cu/NiNiZn-Pd(30s)	1 M KOH	298 K	[27]
Cu/NiNiZn-Au	1 M KOH	298 K	[28]

Table 7: Nickel catalysts reported by Herraiz-Cardona *et al.*

These results show a high degree of agreement, especially when it is considered that the Herraiz-Cardona *et al.* measurements were all performed in stronger electrolyte, and at higher temperature. Solmaz *et al.* aged their Cu/NiCuZn coating to 120 hours at a constant $100\,\mathrm{mA\,cm^{-2}}$, and observed a similar increase in activation over this period, which was attributed to a probable removal of material from the pores. It is not possible to perform comparisons for OER, as to our knowledge these experiments were not reported.

7. Conclusions

This paper presents for the first time a simple modification to the procedure for the electrodeposition of Raney nickel that enhances not just its electrical performance for alkaline water-splitting, but also its lifetime. The performance of the Raney 2 coating for both the hydrogen and oxygen evolution reactions is such that it easily grade stainless steel (316SS), has transformed the coating and permitted it to break new ground in this area of research. It is possible that the new coating is thus a hybrid, able to combine the advantageous properties of both materials, creating a new coating that is effectively 'Stainless Raney nickel'.

The choice of a 316SS counter-electrode that corrodes during deposition will inevitably have affected the constituents of the finished coating, since 316SS contains a variety of elements, most notably Fe, Cr, Mo and (according to our analysis) Cu. Interestingly no Mo at all was detected in the EDX results, which implies that it remained in solution, but Fe was co-deposited, and is well-known for enhancing the catalytic activity of Nickel, especially towards OER[54]. In fact, even the levels at which Fe is present as a contaminant in many laboratory-grade chemicals has been known to bring about a 10-fold increase in activity[55].

Most significantly the choice of counter-electrode appears to have dramatically altered the morphology of the coating from a cracked appearance [11, 22], to a more cauliflower-like appearance (as shown in Figure 9). This morphology change is confirmed to be associated with a marked increase in electrochemical surface area (ECSA).

Similarly, although the standard Raney 1 coating is observed to improve its performance with normal usage, either as anode or cathode, the new Raney 2 coating is observed to improve its performance by an even greater amount. This performance increase is also associated with large increases in the ECSA, a surface area that the coating is able to utilise even up to large current densities where mass-transport issues would be expected. This appears to occur whether zinc continues to be leached out (at the cathode) or not (at the anode). However, it is expected from work by Divisek *et al.* that once the level of zinc falls below about 10 wt% the cathodic overpotential should begin to increase by up to approximately 200 mV[34]. This effect has not been observed in this study, even though cathodic levels of zinc were observed to fall to approximately 2 at%. This disparity could possibly be explained by the difference in the method of assessing the level of zinc, which in the work by Divisek *et al.* was assessed by complexometry (a bulk analytical technique), whereas in this work was assessed by EDX (a non-invasive surface technique). It is quite possible that the low bulk concentrations of zinc reported by Divisek *et al.* were associated with an almost complete absence of zinc at the surface.

A further explanation may rest with the issue of copper contamination, which cannot be ruled out as a contributory factor. Although it is not a common topic of research in the literature in combination with nickel electrodes, in work by Ngamlerdpokin *et al.* all Ni-Cu alloys were observed to have higher electrocatalytic activity for

Journal Pre-proof

poisoning of electrodes is of great concern from a commercial perspective. Finally, it is the hope of the authors that the accelerated ageing tests here outlined will constitute a new and useful benchmark for future comparisons between new electrode materials, thereby condensing the work of months or years into just one week.

Funding. PhD student William Gannon, funded by a University of Swansea Zienkiewicz Scholarship.

Conflicts of Interest. The authors declare no conflict of interest.

References

[1] D. L. Chandler, Vast amounts of solar energy radiate to the Earth, Tech. rep., MIT (2011).
URL http://news.mit.edu/2011/energy-scale-part3-1026

[2] G. S. Pawar, A. A. Tahir, Unbiased Spontaneous Solar Fuel Production using Stable la FeO3 Photoelectrode, Scientific Reports 8 (1) (2018) 1–9. doi:10.1038/s41598-018-21821-z.

[3] P. Chatchai, Y. Murakami, S. ya Kishioka, A. Y. Nosaka, Y. Nosaka, Efficient photocatalytic activity of water oxidation over WO3/BiVO4 composite under visible light irradiation, Electrochimica Acta 54 (3) (2009) 1147–1152. doi:10.1016/j.electacta.2008.08.058.

[4] J. Gong, Y. Lai, C. Lin, Electrochemically multi-anodized TiO2 nanotube arrays for enhancing hydrogen generation by photoelectrocatalytic water splitting, Electrochimica Acta 55 (16) (2010) 4776–4782. doi:10.1016/j.electacta.2010.03.055.

[5] N. Liu, S. P. Albu, K. Lee, S. So, P. Schmuki, Water annealing and other low temperature treatments of anodic TiO 2 nanotubes: A comparison of properties and efficiencies in dye sensitized solar cells and for water splitting, Electrochimica Acta 82 (2012) 98–102. doi:10.1016/j.electacta.2012.06.006.

[6] X. Ding, Y. Gao, L. Zhang, Z. Yu, J. Liu, L. Sun, Artificial photosynthesis: A two-electrode photoelectrochemical cell for light driven water oxidation with molecular components, Electrochimica Acta 149 (2014) 337–340. doi:10.1016/j.electacta.2014.10.111.

[7] J. A. Rudd, M. K. Brennaman, K. E. Michaux, D. L. Ashford, R. W. Murray, T. J. Meyer, Synthesis, Electrochemistry, and Excited-State Properties of Three Ru(II) Quaterpyridine Complexes, Journal of Physical Chemistry A 120 (11) (2016) 1845–1852. doi:10.1021/acs.jpca.6b00317.

[8] R. Phillips, A. Edwards, B. Rome, D. R. Jones, C. W. Dunnill, Minimising the ohmic resistance of an alkaline electrolysis cell through effective cell design, International Journal of Hydrogen Energy 42 (38) (2017) 23986–23994. doi:10.1016/j.ijhydene.2017.07.184.

[9] R. Phillips, C. W. Dunnill, Zero gap alkaline electrolysis cell design for renewable energy storage as hydrogen gas, RSC Advances 6 (102) (2016) 100643–100651. doi:10.1039/C6RA22242K.

[10] F. Gutiérrez-Martín, D. Confente, I. Guerra, Management of variable electricity loads in wind - Hydrogen systems: The case of a Spanish wind farm, International Journal of Hydrogen Energy 35 (14) (2010) 7329–7336. doi:10.1016/j.ijhydene.2010.04.181.

[11] I. Herraiz-Cardona, E. Ortega, V. Pérez-Herranz, Impedance study of hydrogen evolution on Ni/Zn and Ni-Co/Zn stainless steel based electrodeposits, Electrochimica Acta 56 (3) (2011) 1308–1315. doi:10.1016/j.electacta.2010.10.093.

Nickel Institute (2014).
URL https://www.nickelinstitute.org/media/2323/nph_141015.pdf

[14] E. Endoh, H. Otouma, T. Morimoto, Y. Oda, New Raney nickel composite-coated electrode for hydrogen evolution, International Journal of Hydrogen Energy 12 (7) (1987) 473–479. doi:10.1016/0360-3199(87)90044-9.

[15] J. Balej, J. Divisek, H. Schmitz, J. Mergel, Preparation and properties of raney nickel electrodes on Ni-Zn base for H2 and O2 evolution from alkaline solutions Part I: electrodeposition of Ni-Zn alloys from chloride solutions, Journal of Applied Electrochemistry 22 (8) (1992) 705–710. doi:10.1007/bf01027497.

[16] J. Balej, J. Divisek, H. Schmitz, J. Mergel, Preparation and properties of raney nickel electrodes on Ni-Zn base for H2 and O2 evolution from alkaline solutions Part I: electrodeposition of Ni-Zn alloys from chloride solutions, Journal of Applied Electrochemistry 22 (8) (1992) 705–710. doi:10.1007/BF01027497.

[17] C. A. Marozzi, A. C. Chialvo, Development of electrode morphologies of interest in electrocatalysis. Part 1: Electrodeposited porous nickel electrodes, Electrochimica Acta 45 (13) (2000) 2111–2120. doi:10.1016/S0013-4686(99)00422-3.

[18] L. Birry, A. Lasia, Studies of the hydrogen evolution reaction on Raney nickel–molybdenum electrodes, Journal of Applied Electrochemistry 34 (2004) 735–749.

[19] J. Divisek, P. Malinowski, J. Mergel, H. Schmitz, Improved components for advanced alkaline water electrolysis, International Journal of Hydrogen Energy 13 (3) (1988) 141–150. doi:10.1016/0360-3199(88)90014-6.

[20] G. Sheela, M. Pushpavanam, S. Pushpavanam, Zinc-nickel alloy electrodeposits for water electrolysis, International Journal of Hydrogen Energy 27 (6) (2002) 627–633. doi:10.1016/S0360-3199(01)00170-7.

[21] I. Herraiz-Cardona, E. Ortega, L. Vázquez-Gómez, V. Pérez-Herranz, Electrochemical characterization of a NiCo/Zn cathode for hydrogen generation, International Journal of Hydrogen Energy 36 (18) (2011) 11578–11587. doi:10.1016/j.ijhydene.2011.06.067.

[22] I. Herraiz-Cardona, C. González-Buch, C. Valero-Vidal, E. Ortega, V. Pérez-Herranz, Co-modification of Ni-based type Raney electrodeposits for hydrogen evolution reaction in alkaline media, Journal of Power Sources 240 (2013) 698–704. doi:10.1016/j.jpowsour.2013.05.041.

[23] C. González-Buch, I. Herraiz-Cardona, E. Ortega, J. García-Antón, V. Pérez-Herranz, Synthesis and characterization of macroporous Ni, Co and Ni-Co electrocatalytic deposits for hydrogen evolution reaction in alkaline media, International Journal of Hydrogen Energy 38 (25) (2013) 10157–10169. doi:10.1016/j.ijhydene.2013.06.016.

[24] R. Solmaz, A. Döner, G. Kardaş, Preparation, characterization and application of alkaline leached CuNiZn ternary coatings for long-term electrolysis in alkaline solution, International Journal of Hydrogen Energy 35 (19) (2010) 10045–10049. doi:10.1016/j.ijhydene.2010.07.145.

[25] R. Solmaz, Electrochemical preparation, characterization, and application of a novel cathode material, mild Steel/Ni/NiZn-Pt, for alkaline water electrolysis, Energy Sources, Part A: Recovery, Utilization and Environmental Effects 36 (11) (2014) 1212–1218. doi:10.1080/15567036.2010.545804.

[26] R. Solmaz, A. Döner, M. Doğrubaş, I. Y. Erdoğan, G. Kardaş, Enhancement of electrochemical activity of Raney-type NiZn coatings by modifying with PtRu binary deposits: Application for alkaline water electrolysis, International Journal of Hydrogen Energy 41 (3) (2016) 1432–1440. doi:10.1016/j.ijhydene.2015.11.027.

[27] R. Solmaz, A. Salcı, H. Yüksel, M. Doğrubaş, G. Kardaş, Preparation and characterization of Pd-modified Raney-type NiZn

Journal Pre-proof

Research 41 (2017) 1452–1459.

[29] J. Balej, Electrocatalysts for oxygen evolution in advanced water electrolysis, International Journal of Hydrogen Energy 10 (2) (1985) 89–99. doi:10.1016/0360-3199(85)90041-2.

[30] M. K. Bates, Q. Jia, H. Doan, W. Liang, S. Mukerjee, Charge-Transfer Effects in Ni-Fe and Ni-Fe-Co Mixed-Metal Oxides for the Alkaline Oxygen Evolution Reaction, ACS Catalysis 6 (1) (2016) 155–161. doi:10.1021/acscatal.5b01481.

[31] C. Bourasseau, B. Guinot, Hydrogen Production (Chapter 8) "Hydrogen: A Storage Means for Renewable Energies", Wiley, 2015.

[32] W. Gannon, D. Jones, C. Dunnill, Enhanced Lifetime Cathode for Alkaline Electrolysis Using Standard Commercial Titanium Nitride Coatings, Processes 7 (2) (2019) 112. doi:10.3390/pr7020112.

[33] J. Divisek, H. Schmitz, B. Steffen, Electrocatalyst Materials Evolution for Hydrogen, Electrochimica Acta 39 (11) (1994) 1723–1731.

[34] J.Divisek, J.Mergel, H.Schmitz, Advanced Water Electrolysis and Catalyst Stability under Discontinuous Operation, International Journal of Hydrogen Energy 15 (2) (1990) 105–114. doi:10.1016/0360-3199(90)90032-T.

[35] F. M. Sapountzi, J. M. Gracia, C. K.-J. Weststrate, H. O. Fredriksson, J. H. Niemantsverdriet, Electrocatalysts for the generation of hydrogen, oxygen and synthesis gas, Progress in Energy and Combustion Science 58 (2017) 1–35. doi:10.1016/j.pecs.2016.09.001.

[36] M. P. Marceta Kaninski, V. M. Nikolic, G. S. Tasic, Z. L. Rakocevic, Electrocatalytic activation of Ni electrode for hydrogen production by electrodeposition of Co and V species, International Journal of Hydrogen Energy 34 (2) (2009) 703–709. doi:10.1016/j.ijhydene.2008.09.024.
URL `http://dx.doi.org/10.1016/j.ijhydene.2008.09.024`

[37] Y. P. Zhu, Y. P. Liu, T. Z. Ren, Z. Y. Yuan, Self-supported cobalt phosphide mesoporous nanorod arrays: A flexible and bifunctional electrode for highly active electrocatalytic water reduction and oxidation, Advanced Functional Materials 25 (47) (2015) 7337–7347. arXiv:0706.1062v1, doi:10.1002/adfm.201503666.

[38] H. Dong, T. Lei, Y. He, N. Xu, B. Huang, C. T. Liu, Electrochemical performance of porous Ni3Al electrodes for hydrogen evolution reaction, International Journal of Hydrogen Energy 36 (19) (2011) 12112–12120. doi:10.1016/j.ijhydene.2011.06.115.

[39] Z. W. Seh, J. Kibsgaard, C. F. Dickens, I. Chorkendorff, J. K. Nørskov, T. F. Jaramillo, Combining theory and experiment in electrocatalysis: Insights into materials design, Science 355 (6321) (2017) eaad4998. doi:10.1126/science.aad4998.

[40] T. Shinagawa, A. T. Garcia-esparza, K. Takanabe, Insight on Tafel slopes from a microkinetic analysis of aqueous electrocatalysis for energy conversion, Nature Publishing Group 5 (May). doi:10.1038/srep13801.

[41] O. Diaz-Morales, D. Ferrus-Suspedra, M. T. M. Koper, The importance of nickel oxyhydroxide deprotonation on its activity towards electrochemical water oxidation, Chem. Sci. 7 (4) (2016) 2639–2645. doi:10.1039/C5SC04486C.

[42] C. C. L. McCrory, S. Jung, I. M. Ferrer, S. M. Chatman, J. C. Peters, T. F. Jaramillo, Benchmarking HER and OER Electrocatalysts for Solar Water Splitting Devices - SI, J. Am. Chem. Soc. 137 (13) (2015) 4347–4357. doi:10.1021/ja510442p.

[43] C. C. L. McCrory, S. Jung, I. M. Ferrer, S. M. Chatman, J. C. Peters, T. F. Jaramillo, Benchmarking Hydrogen Evolving Reaction and Oxygen Evolving Reaction Electrocatalysts for Solar Water Splitting Devices, Journal of the American Chemical Society 137 (13) (2015) 4347–4357. doi:10.1021/ja510442p.

[44] G. Passas, C. W. Dunnill, Water Splitting Test Cell for Renewable Energy Storage as Hydrogen Gas, Fundamentals doi:10.1039/c8cc05896b.

[46] F. Yu, H. Zhou, Y. Huang, J. Sun, F. Qin, J. Bao, W. A. Goddard, S. Chen, Z. Ren, High-performance bifunctional porous non-noble metal phosphide catalyst for overall water splitting, Nature Communications 9 (1) (2018) 1–9. doi:10.1038/s41467-018-04746-z.

[47] N. Jiang, B. You, M. Sheng, Y. Sun, Electrodeposited Cobalt-Phosphorous-Derived Films as Competent Bifunctional Catalysts for Overall Water Splitting, Angewandte Chemie - International Edition 54 (21) (2015) 6251–6254. doi:10.1002/anie.201501616.

[48] H. Wang, H. W. Lee, Y. Deng, Z. Lu, P. C. Hsu, Y. Liu, D. Lin, Y. Cui, Bifunctional non-noble metal oxide nanoparticle electrocatalysts through lithium-induced conversion for overall water splitting, Nature Communications 6 (2015) 1–8. doi:10.1038/ncomms8261.
URL `http://dx.doi.org/10.1038/ncomms8261`

[49] L. Jiao, Y. X. Zhou, H. L. Jiang, Metal-organic framework-based CoP/reduced graphene oxide: High-performance bifunctional electrocatalyst for overall water splitting, Chemical Science 7 (3) (2016) 1690–1695. doi:10.1039/c5sc04425a.

[50] Y. Li, H. Zhang, M. Jiang, Y. Kuang, X. Sun, X. Duan, Ternary NiCoP nanosheet arrays: An excellent bifunctional catalyst for alkaline overall water splitting, Nano Research 9 (8) (2016) 2251–2259. doi:10.1007/s12274-016-1112-z.

[51] C. Tang, N. Cheng, Z. Pu, W. Xing, X. Sun, NiSe Nanowire Film Supported on Nickel Foam: An Efficient and Stable 3D Bifunctional Electrode for Full Water Splitting, Angewandte Chemie - International Edition 54 (32) (2015) 9351–9355. doi:10.1002/anie.201503407.

[52] W. Zhu, X. Yue, W. Zhang, S. Yu, Y. Zhang, J. Wang, J. Wang, Nickel sulfide microsphere film on Ni foam as an efficient bifunctional electrocatalyst for overall water splitting, Chem. Commun. 52 (7) (2016) 1486–1489. doi:10.1039/C5CC08064A.

[53] I. Herraiz-Cardona, E. Ortega, J. G. Antón, V. Pérez-Herranz, Assessment of the roughness factor effect and the intrinsic catalytic activity for hydrogen evolution reaction on Ni-based electrodeposits, International Journal of Hydrogen Energy 36 (16) (2011) 9428–9438. doi:10.1016/j.ijhydene.2011.05.047.

[54] E. Fabbri, A. Habereder, K. Waltar, R. Kötz, T. J. Schmidt, R. Kotz, T. J. Schmidt, Developments and perspectives of oxide-based catalysts for the oxygen evolution reaction, Catalysis Science & Technology 4 (11) (2014) 3800–3821. doi:10.1039/C4CY00669K.

[55] A. M. Smith, L. Trotochaud, M. S. Burke, S. W. Boettcher, Contributions to activity enhancement via Fe incorporation in Ni-(oxy)hydroxide/borate catalysts for near-neutral pH oxygen evolution, Chemical Communications 51 (25) (2015) 5261–5263. doi:10.1039/c4cc08670h.

[56] K. Ngamlerdpokin, N. Tantavichet, Electrodeposition of nickel-copper alloys to use as a cathode for hydrogen evolution in an alkaline media, International Journal of Hydrogen Energy 39 (6) (2014) 2505–2515. doi:10.1016/j.ijhydene.2013.12.013.

Journal Pre-proof

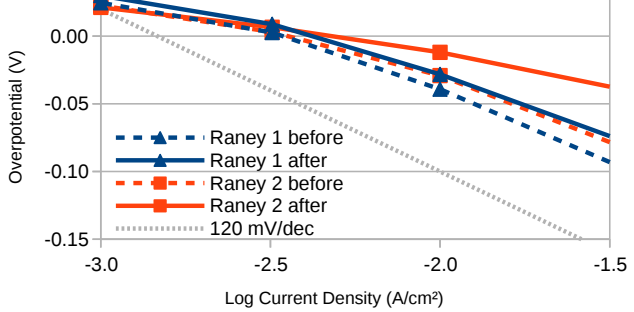

Figure S1: Detail view of Figure 8 showing just Raney 1 and 2 before and after accelerated ageing

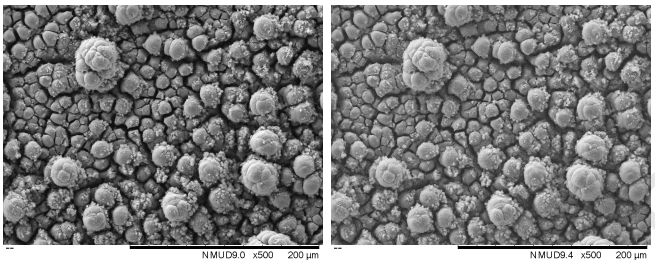

(a) As deposited (b) After ageing

Figure S2: SEM images of Raney 2 at 500× magnification before and after accelerated ageing as anode

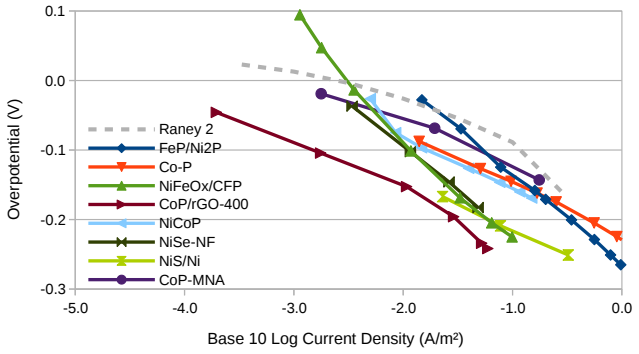

Figure S3: Raney 2 bifunctional comparisons for HER

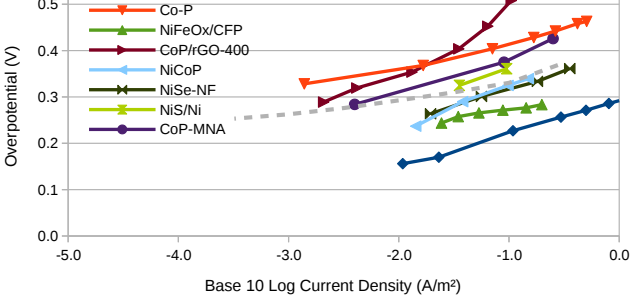

Figure S4: Raney 2 bifunctional comparisons for OER

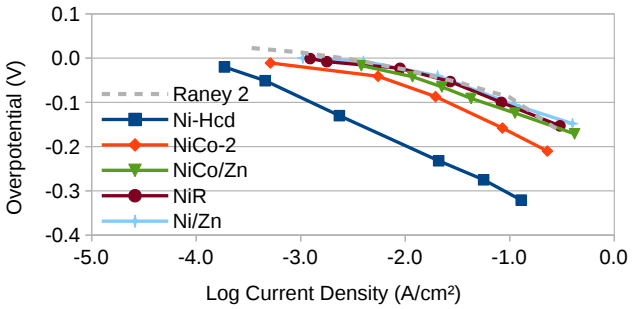

Figure S5: Comparisons with the coatings of Herraiz-Cardona *et al* listed in Table 7

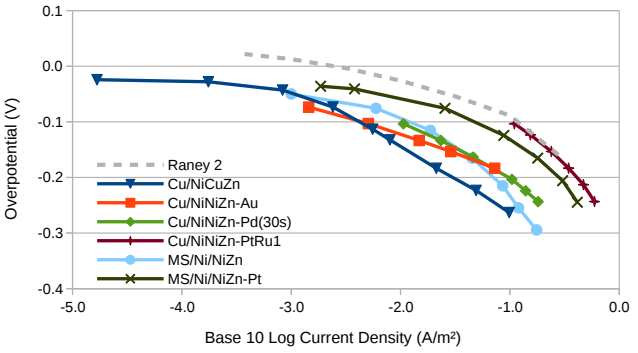

Figure S6: Comparisons with the coatings of Solmaz *et al* listed in Table 7

Journal Pre-proof